CAMBRIDGE
UNIVERSITY PRESS

RESEARCH ARTICLE

Development of a seat support mechanism for guiding users to an appropriate posture in a seated-style echocardiography robot

Yuuki Shida[1] , Mayu Morita[2], Tetsunori Shiotani[3] and Hiroyasu Iwata[4]

[1]Graduate School of Creative Science and Engineering, Waseda University, Tokyo, Japan
[2]School of Creative Science and Engineering, Waseda University, Tokyo, Japan
[3]Graduate School of Advanced Science and Engineering, Waseda University, Tokyo, Japan
[4]Faculty of Science and Engineering, Waseda University, Tokyo, Japan
Corresponding author: Yuuki Shida; Email: arares201@moegi.waseda.jp

Abstract

This paper proposes a seat support mechanism to solve the problem of misalignment between the chest examination and probe scanning areas when the patient is bent in a seated-style echocardiography robot. To guide the patient to an appropriate body position where their chest is within the examination range of the chest examination unit while minimizing the physical load of the patient, the posture of the patient must satisfy the three following conditions. (i) The breech must be in contact with the seat surface, (ii) the legs must be vertical to the floor, and (iii) the chest and mechanism must be parallel while the probe scanning and chest examination ranges must match. The human body was modeled to derive a posture that satisfies the aforementioned conditions for the height of each individual, and a seat support mechanism with four degrees of freedom was installed to guide the user to the derived posture. By installing this mechanism, the body load of the left biceps brachii, right biceps brachii, left latissimus dorsi, and right latissimus dorsi was reduced to 64.7%, 52.7%, 86.4%, and 80.2%, respectively. The sharpness of the image contours was improved to 103.8%.

1. Introduction

Heart disease is the deadliest in the world, leading to the demise of 17.9 million people in 2019 [1]. Thus, periodic health checkups using transthoracic echocardiography (TTE), which accelerates the early detection of cardiac disease, have attracted attention. In TTE in medical practice, the patient's posture is first adjusted so that clear ultrasound (US) images of the heart can be acquired, according to individual differences in the patient's body shape and build. Next, the position and angle of the probe are adjusted to acquire the basic views necessary for diagnosis. Finally, multiple acquired basic views are used to determine the presence or absence of heart disease [2]. US examinations, including TTE, are difficult because these processes require a high degree of skill and experience for the physician and technologist to manipulate the US probe while maintaining hand-eye coordination. Owing to the required number of skills, there are insufficient sonographers. Various assistive technologies for robotic-based US examinations have been developed to solve the aforementioned problems. These robots are focused on several applications, including the carotid, liver, fetal echocardiography, cardiac tamponade, lung, and other generic sites [3–16]. However, in TTE, there are lungs and ribs between the chest and the heart that reflect and absorb US, making it difficult to obtain clear US images. The heart is an organ whose position in the body shifts with lateral bending and forward bending of the body. To obtain clear US images, it is necessary to adjust the patient's posture and position the heart in a position that is less affected by the lungs and ribs. Although the robot for TTE requires an inspection unit to move the probe
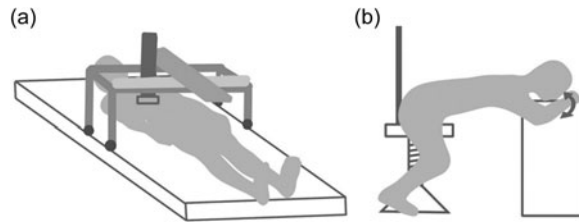
Figure 1. *Echocardiography robot and subject placement (a) supine (b) seated.*
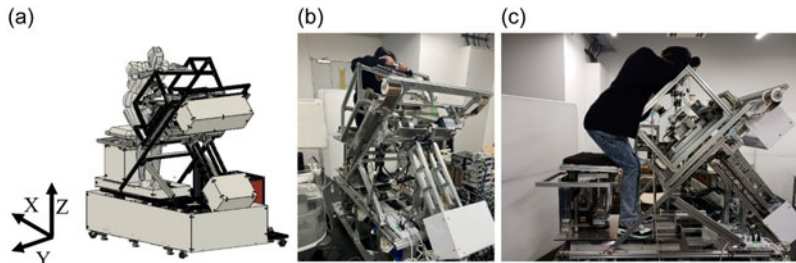

Figure 2. *Seated-style echocardiography robot. (a) Overall view (b) Patient during an examination.*

and a diagnostic posture control system to adjust the posture, previous studies did not include the latter, making robotic TTE difficult.

Because of the difficulty of the problem, research on robots for TTE has been dominated by studies on telemedicine robots that can adjust the position and posture of the patient and probe according to the physician's instructions [17–19] and studies that analyze the US date acquired by the physician to assist in the diagnosis of disease [20–22], and only a few studies have focused on robots for TTE [23,24]. These robots perform examinations in the supine position. Although they can perform examinations in the conventional examination posture in medical settings, they lack emergency evacuation and cause high patient anxiety (Figure 1(a)). On the other hand, it is unclear whether the robot can perform medical diagnosis by examining the patient in the sitting posture as in the conventional method, but it can guarantee emergency evacuation and provide a sense of security (Figure 1(b)). Thus, the authors developed a diagnostic posture control system to realize a seated-style echocardiography robot after verifying the feasibility of echocardiographic examinations in the sitting posture [24]. This system enables patients to undergo echocardiographic examinations in a seated posture, and the robot does not cover the patient. Thus, the system is superior in terms of safety and emergency evacuation. The proposed system comprises three and two active and passive degrees of freedom (DOFs), respectively, allowing the system to be controlled to any posture angle (Figure 2(a)). Also, as a device to reduce the physical load, the angle of the base on which the patient's feet are placed on this robot follows and tilts in accordance with the lateral bending angle of the patient's body, enabling the patients to support their bodies by distributing the force evenly to both feet, thereby reducing the burden on the legs.

However, the scanning range of the chest of the patient and that of the robot probe are misaligned when the patient flexes their posture. To eliminate this misalignment, the patient is placed in a posture that is physically demanding to maintain, such as sitting shallowly on the seat or floating at the lower back (Figure 2(b)). The patient maintains their posture by the force of the arms holding the robot handles and the force of the lower back. This places a burden on the arms and lower back. This unstable posture prevents the chest from making proper contact with the probe, which may result in poor image quality. CT and MRI are medical devices that adjust the patient's position and examine the inside of the body. CT uses X-rays and MRI uses magnetic fields to read body information, which are less susceptible to interference by body organs than US. Therefore, the patient's posture does not need to be adjusted more
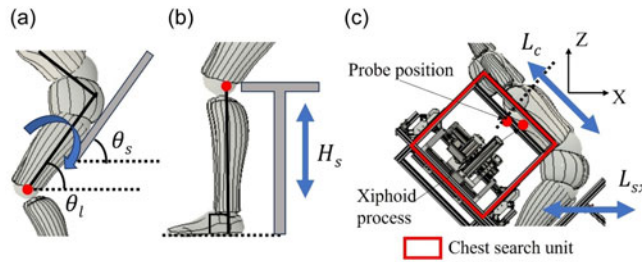
Figure 3. *Role of each function of the seat support mechanism. (a) Seat tilting mechanism. (b) Seat lifting mechanism. (c) Seat sliding mechanism and probe position-adjusting mechanism.*

precisely than in ultrasonography, making it difficult to use this device in a TTE robot. Thus, there is no body support mechanism that has the dual function of adjusting the examination site of the robot to the patient's posture to be adjusted for the examination and supporting the patient to minimize the patient's body load. This paper proposes a seat support mechanism that guides the patient to an appropriate body position while maintaining leg load and reducing arm and lower back load. Note that the coordinate axes are defined as shown in Figure 2(a).

2. Method

2.1. Design requirement

The seat support mechanism must be able to (i) not impose any physical burden on the patient to maintain the posture, (ii) allow the patient to get in and out quickly and not feel restrained, and (iii) guide the patient into a posture that allows accurate diagnosis. A posture that satisfies this requirement is defined as an appropriate posture in this paper. Three restraint conditions were necessary to guide the robot into a posture that satisfies these requirements. (1) The chest examination and probe scanning ranges coincide without any burden to the patient when the posture is flexed, and (2) the emergency evacuation capability of the robot is ensured. The three constraints are that (I) the breech is in contact with the seat surface, (II) the feet (lower legs) are perpendicular to the ground, and (III) the chest examination and probe scanning areas coincide (Figure 3). Condition I allows the patient to maintain their posture because of the normal force of the seat surface, thereby reducing the burden of maintaining the posture on the arms and lower back. Condition II enables the legs to easily apply force when supporting the posture, and the vertical attachment of the legs allows for immediate evacuation in an emergency.

The mechanisms necessary to satisfy these constraints are proposed. First, to satisfy all the constraints and realize requirement i, the legs must remain perpendicular to the ground and the chest must be flexed in the examination posture. To achieve this, it is necessary to have a feature that induces changes in the angle of the knee joint while inclining the seat surface according to the angle of the hip joint, ensuring that the buttocks come into contact with the seat surface. This function can be achieved by raising the breech forward. Specifically, a seat tilting mechanism that changes the angle of the seat surface is introduced (Figure 3(a)). Next, the height of the seat surface must match the length of the lower leg for the legs to contact the ground vertically, which satisfies constraint II and realizes requirements i and ii. To achieve this, a seat lifting mechanism that changes the height of the seat surface, H_s, is introduced (Figure 3(b)). Finally, for constraint condition III and realize requirement iii, it is necessary to eliminate the misalignment between the inspection area of the chest and the probe scanning area. The misalignment is two-dimensional in the X- and Z-axis directions. Thus, two mechanisms must be introduced to adjust the chest position of the patient: a seat sliding mechanism to move the seat portion to the front-back position, L_{sx}, and a probe position-adjusting mechanism to raise or lower the position, L_c, of the chest unit equipped with the probe scanning mechanism (Figure 3(c)). Here, the initial position of the probe of the robot coinciding with the xiphoid process of the patient is defined as the position of the chest search
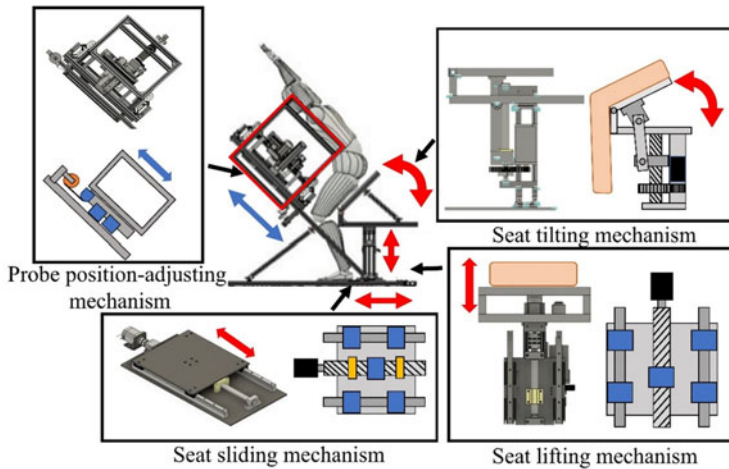
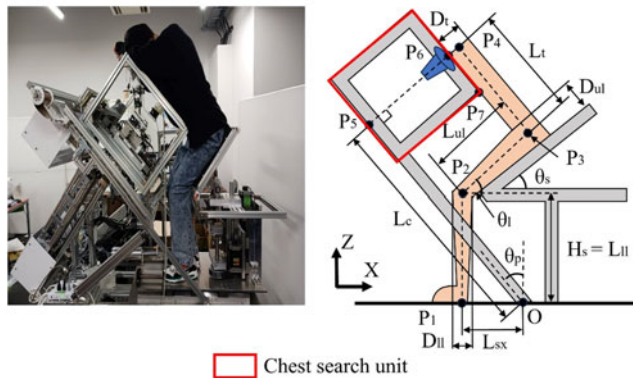**Figure 4.** *Overview of seat support mechanism.*

Figure 5. *A simplified model of a passenger in a seat support mechanism.*

unit and the chest, which complies with the method of automated robotic echocardiography described in Ref. [25].

The seat support mechanism automatically moves and adjusts its position according to the subject's height before the subject gets on the seat, and the subject gets on the seat support mechanism after the adjustment. The seat support mechanism does not move after the subject gets on the seat. Thus, to ensure the safety of the subject, it is not necessary to consider the speed of actuator movement, but rather to consider the following two points: (i) the seat support mechanism must maintain the posture even if the motor stops in the event of an emergency stop or power failure, and (ii) the subject must be able to easily dismount by himself immediately in the event of an emergency. Figure 4 shows an overview of the seat support mechanism integrating these functions. The parameters of these mechanisms are determined in Sec. 2-2. The details of these mechanisms are described in Sec. 2-3.

2.2. Identification of the parameters of the seat support mechanism

The purpose of this section is to derive each parameter θ_s, H_s, L_{sx}, and L_c of the seat support mechanism to guide the patient to the appropriate posture described in the previous section. First, a simple model of the patient is placed on the robot to satisfy the two constraint conditions in the previous section, II: the feet (lower legs) are perpendicular to the ground, and III: the chest examination and probe scanning areas coincide (Figure 5). Next, the parameters of the seat support mechanism are derived to satisfy the

***Table I.*** *Definitions of the variables used in Figure 5 and Figure 6(a).*

Variable name	Description	Variable name	Description
P_1 to P_2	Lower leg	L_{sx}	Length from origin O to patient's sole = X-coordinate of P_1
P_2 to P_3	Upper leg	L_{56}	Length between P5 and P6
P_3	Hip joint	L_{bc}	Length of P_1 and P_{bc} in X-axis direction
P_4	Xiphoid process	D_{ll}	Diameter of lower leg
P_5	Intersection of perpendicular lines drawn from the initial position of the probe to the side of the chest search unit opposite the side in contact with the chest	D_{ul}	Diameter of upper leg
P_6	Initial position of probe	D_t	Diameter of torso
P_7	Lower end of chest search unit	H_s	Height of the seat surface
P_h	Position of the hand grasp	θ_1	Angle between upper thigh and horizontal axis
P_{bc}	Position of the patient's body center of gravity	θ_p	Fllexion angle of robot
P_s	Position of normal force on the seat surface	θ_s	Angle between seat surface and horizontal axis
L_{ll}	Length of lower leg	F_h	Force supported by hands and lower back
L_{ul}	Length of upper leg	F_l	Force in Z-axis direction applied to legs
L_t	Distance from hip joint to xiphoid process	F_s	Normal force on the seat surface
L_c	Length from origin O to chest search unit	Mg	Patient's gravity

restraint condition described in the previous section, I: the breech is in contact with the seat surface, in order to minimize the physical burden on the patient. Finally, how the body load on the arms, waist, and legs is affected by the introduction of the seat support mechanism is derived. A detailed description of these processes is provided below.

First, the values of each variable in the patient's model are calculated. The definitions of the variables used in Figure 5 are shown in Table I. Note that θ_p is a value adjusted and determined for each individual patient so that US images of the heart can be clearly visualized in echocardiography [24]. The body parameters $P = L_{ll}, L_{ul}, L_t, D_{ll}, D_{ul}$, and D_t of the patient using the seat support mechanism were calculated using Eq. (1) with the mean values of each parameter $\overline{P}$ and height $\overline{H}$, Height H. The mean values of each parameter $\overline{P}$ and height $\overline{H}$ were calculated from Ref. [26]. Note that $\overline{P}$ is the mean value of each parameter, $\overline{H}$ is the mean value of height, and H is the height of the patient using the seat support mechanism. The mean of each parameter and height are derived from a data set Ref. [26] with a population of 3530 men between 19.5 and 79.5 years of age. The mean values of each parameter are L_{ll}: 446.1 cm, L_{ul}: 409.5 cm, L_t: 286.4 cm, D_{ll}: 118.7 cm, D_{ul}: 179.2 cm, and D_t: 219.1 cm, respectively.

$$P = \overline{P}\frac{H}{\overline{H}} \tag{1}$$

Next, each parameter of the seat support mechanism is derived. In the model, the constraints in conditions II and III were synonymous with the following. Condition II: P_1P_2 and the floor are perpendicular.
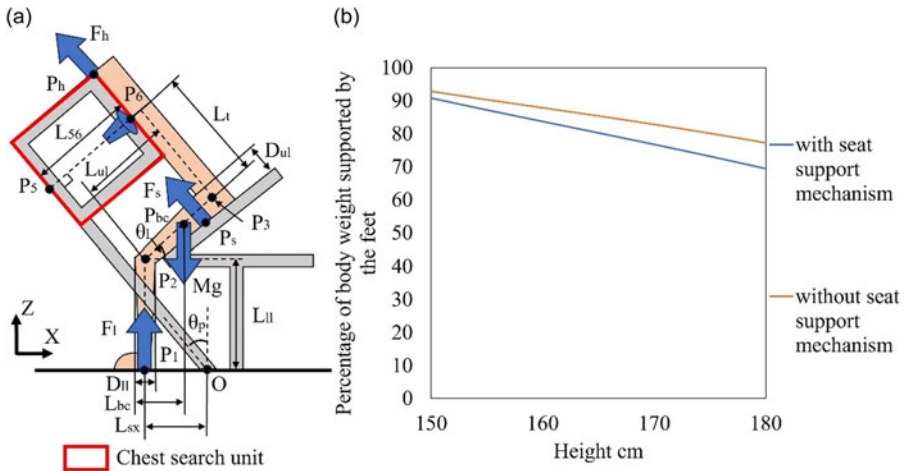
Figure 6. *Analysis of load reduction in each part by seat support mechanism (a) free body diagram for the forces applied between the seat support mechanism and the patient's body (b) ratio of legs support to body weight in each condition for each height.*

Condition III: P_3P_4 and P_6P_7 are parallel, the distance between P_3P_4 and P_6P_7 is $D_t/2$, and P_4 is an extension of line segment P_5P_6. Condition I is satisfied by deriving θ_s, which satisfies it according to the lower and upper leg angles, θ_1, of the patient calculated by satisfying conditions II and III. θ_1, θ_s, H_s, L_{sx}, and L_c were identified with each parameter from these constraints, resulting in Eqs. (2), (3), (4), (5), and (6), respectively.

$$\theta_l = \sin^{-1}\left[\frac{\{2L_{ll}\left(\cos\theta_p - 1\right) + (2L_{56} + D_t)\sin\theta_p\}}{2L_{ul}}\right] \tag{2}$$

$$\theta_s = \theta_l + \tan^{-1}\frac{D_{ll} - D_{ul}}{2L_{ul}}. \tag{3}$$

$$H_s = L_{ll} \tag{4}$$

$$L_{sx} = \left(L_{56} + \frac{D_t + D_{ll}}{2}\right)\cos\theta_p - L_{ll}\sin\theta_p - L_{ul}\cos\theta_l. \tag{5}$$

$$L_c = L_{ll} + L_t \tag{6}$$

Finally, it is analyzed how the seat support mechanism reduces the load on the arms, lower back, and legs by using a free body diagram (FBD). The FBD for the forces applied between the seat support mechanism and the patient's body are shown in Figure 6(a). The definitions of the variables used in Figure 6(a) are shown in Table I. Eqs. (7) and (8) show the equations for the equilibrium of moments around P_1 and the equation for the equilibrium of forces in the Z-axis direction.

$$F_h\left(L_{56} + L_{sx}\cos\theta_p\right) + F_s\left\{L_{ll}\sin\theta_l + L_{ul}\frac{D_{ll} + 2D_{ul}}{3\left(D_{ll} + D_{ul}\right)}\right\} = MgL_{bc} \tag{7}$$

$$F_l = Mg - F_h\cos\theta_p - F_s\cos\theta_l \tag{8}$$
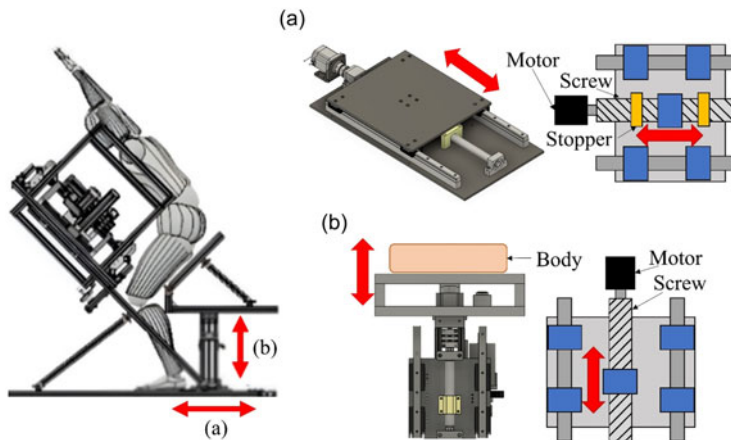
Figure 7. *(a) Seat sliding and (b) lifting mechanisms.*

From Equation **7**, $F_s = 0$ when there is no seat support mechanism, and F_h, the force of the arms and lower back, must be increased to support the body, but when the hip is supported by the seat support mechanism ($F_s > 0$), F_h can be reduced, and the burden on the arms and lower back can be reduced.

The leg load was compared in two conditions: Condition A: without seat support mechanism, and Condition B: with seat support mechanism, when it is possible to support with half the arm and hip force of the F_h value without seat support mechanism. Figure 6(b) shows the ratio of leg support to body weight in each condition for each height. Note that the pitch angle is 45° and the center of gravity of the body is assumed to be at the center of the upper thigh. From this graph, it can be seen that the load on the legs can be reduced by about 2.0 to 7.8% of the body weight by using the seat support mechanism, but the reduction of the load is slight because about 80% of the body weight is supported by the legs. This suggests that the leg load is maintained or slightly reduced and that the goal of maintaining leg load has been achieved.

2.3. Design detail

The results in the previous section showed that four DOFs were necessary to guide the patient to an appropriate body position and posture. This is such that the chest examination range matches the range of motion of the probe of the robot while the body load of the patient is small: translation of the seat surface in the X- and Z-axis directions, inclination of the seat surface, and translation of the chest search unit. The details of the mechanism to realize these motions are described in this section.

The developed system comprises three active DOFs: i) seat sliding mechanism, ii) seat lifting mechanism, and iii) seat tilting mechanism, as well as one passive DOF and a probe position-adjusting mechanism (Figure 4). The three active degrees of freedom can be accurately and automatically adjusted by controlling the position with a motor equipped with an encoder, and the patient can be automatically guided to the human body posture calculated in the previous section. The position of the chest search unit can be fine-tuned by the patients themselves with one passive degree of freedom, allowing them to adjust to a comfortable posture that is both diagnostic and comfortable.

The seat sliding mechanism controls the translation of the seat surface in the X-axis direction via a linear motion mechanism using a trapezoidal screw (MTSTRW32-900-F100-V25-S30-Q25, MISUMI, Japan) and a stepping motor (PKE599RC2, ORIENTAL MOTOR, Japan). The seat lifting mechanism controls the translation of the seat surface in the Z-axis direction via a linear motion mechanism using a trapezoidal screw (MTSRW28-295-F60-V15-S35-Q15, MISUMI, Japan) and the stepping motor. As shown in Figure 7(a) and 7(b), the seat sliding and lifting mechanisms were operated by moving the
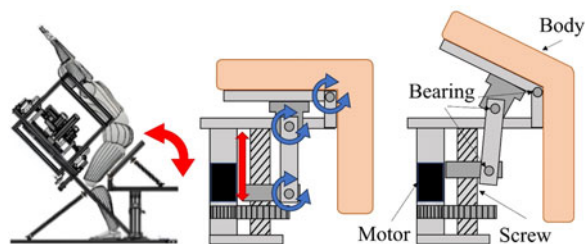
Figure 8. *Seat tilting mechanism.*
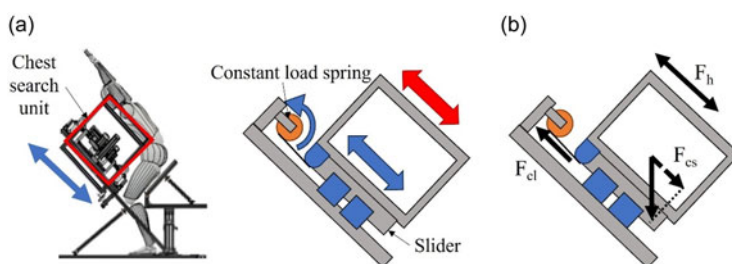
Figure 9. *Probe position-adjusting mechanism (a) overview (b) self-weight compensation mechanism.*

trapezoidal screw thread in the direction of the red arrow. These mechanisms were supported by the trapezoidal screw and two sliders to withstand a load equivalent to the body weight of the patient to allow fine adjustment during the test with the patient on board.

The seat tilting mechanism controls the tilt angle of the seat surface by a four-section linkage mechanism using trapezoidal screws (MTSTRW28-420-F80-V20-S50-Q20, MISUMI, Japan) and stepping motors (PKE5913RC2, ORIENTAL MOTOR, Japan). As shown in Figure 8, the seat tilting mechanism functions by moving the trapezoidal screw unit in the direction of the red arrow. The seat unit is connected to the trapezoidal screw unit via a rotary axis, and the translational motion by the trapezoidal screw is converted into the rotational motion of the seat. The probe position-adjusting mechanism can be manually moved in the direction of the blue arrow (Figure 4) by self-weight compensation using a constant load spring (CR-19, Accurate, Japan) that provides constant tension regardless of the amount of its displacement (Figure 9(a)). In the probe position-adjusting mechanism, the chest search unit is pulled by a constant load spring with an elastic force F_{cl} equal to its gravitational component Fcs. This allows the chest search unit to be moved up and down using only the human hand force F_h (see Figure 9(b)). Also, a handle-type stopper is attached to the slider, allowing the patient to fix the chest search unit in any desired position by himself. This mechanism allows the patients themselves to fine-tune the position of the chest search unit when they find it difficult to align it with their chest.

In terms of safety, as mentioned in the "Design requirement" section, it is necessary to consider the following two points: (i) the seat support mechanism must maintain the posture even if the motor stops in the event of an emergency stop or power failure, and (ii) the subject must be able to easily dismount by himself immediately in the event of an emergency. As for (i), the seat support mechanism uses a trapezoidal screw, which has a self-locking function due to its high friction coefficient and retains its position when the motor stops. This allows the seat support mechanism to maintain the position at which it stopped in the event of a motor failure or power interruption. As for (ii), the probe position-adjusting mechanism allows the subject to move the chest search unit by themselves, and in an emergency, the subject can easily evacuate by lifting the chest search unit.

Table II. *List of conditions for verification of seat support mechanism.*

Condition	Seat support mechanism	Individual variation support
A	Not introduced	–
B	Introduced	Fixed each parameter of the mechanism according to the average male height
C	Introduced	Adjust each parameter of the mechanism according to the height of each individual
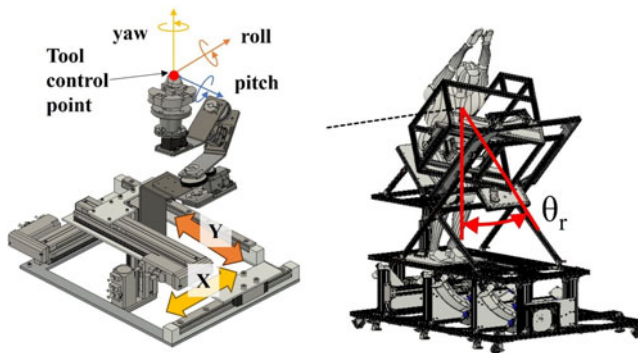
Figure 10. *Definition of probe angle and posture angle of the patient on the robot.*

3. Evaluation

3.1. Experimental setup

To validate the developed seat support mechanism, the following experiments were conducted: (1) verification of physical load reduction and (2) verification of improved clarity of US images and reduction of body displacement. The experiments were performed using the seated-style echocardiography robot [24], a muscle potential measurement device (Wireless EMG system Trigno, 4 Assist, Japan), a motion capture system (V120 Trio, OptiTrack, Japan), a matrix array sector probe (X5-1, Philips, Netherland), and US equipment (EPIQ 7G, Philips, Netherlands). Six subjects were used (height $= 172 \pm 16$ cm). Each experiment was performed with the robot guiding the posture of the subject to θ_r 10° and θ_p 45°. θ_r is 90° minus the angle between the gravity vector and frontal axis (see Figure 10), and θ_p is defined in Table I and Figure 5. Experimental conditions are shown in Table II. Each parameter of the seat support mechanism is calculated using Eqs. (1)–(6) in the Methods chapter. In condition B, the parameters are fixed to those calculated by substituting the average male height into those equations. In condition C, the subject's height was substituted into those equations, and each parameter of the seat support mechanism was adjusted for each individual. The values of each parameter of the seat support mechanism for each subject in conditions B and C are shown in Table III. Condition A and condition C were compared to examine the usefulness of the seat support mechanism, and Condition B and condition C were compared to examine the usefulness of the seat support mechanism's ability to adapt and adjust to the individual's body shape. In this validation test, the probe position-adjusting mechanism was adjusted by the authors to the position derived in the Identification of the parameters of the seat support mechanism section, and the fine-tuning by the patients themselves was not performed.

3.1.1. Verification of physical load reduction

During this experiment, the effectiveness of the proposed seat support mechanism in reducing the body load was quantitatively evaluated by electromyography to verify its validity. The procedure for the experiment is as follows:

Table III. *List of the values of each parameter of the seat support mechanism for each subject in conditions B and C.*

Condition	Subject	Height cm	θ_s deg	H_s cm	L_{sx} deg	L_c deg
B	all		50.9	446.1	−41.4	732.5
	a	156	59.4	413.4	38.0	678.9
	b	163	54.1	432.0	−9.1	709.3
	c	170	49.9	450.6	−51.1	739.8
C	d	172	48.9	455.8	−62.5	748.5
	e	182	44.2	482.4	−116.4	792.0
	f	188	41.9	498.3	−147.0	818.1

(1) Subjects were attached to electromyographs (EMGs) on the left and right biceps brachii, latissimus dorsi, triceps surae, and quadriceps femoris.

(2) The maximum voluntary contraction (MVC) of the biceps brachii, latissimus dorsi, triceps surae, and quadriceps femoris were measured.

(3) The test subjects were seated in a robot adjusted to each condition shown in Table II. The subjects were made to maintain a posture where the probe hits the xiphoid process for 30 s. During this time, the electromyographic activity of each body part was measured. Measurements were taken once for each condition.

(4) A band-pass filter with a cutoff frequency of 20 and 450 Hz was applied to the EMGs acquired under each condition, and the signal envelope using the root mean square of a 300-ms moving slit was extracted. This process was performed following Ref. [27].

(5) The %MVC (the ratio of the EMG value to the maximum EMG value when the most force was applied at each site) was calculated from the median of the values calculated in (4) and the MVC obtained in (2) and was used as the representative value for each condition. The body load of each part of the body under each condition was compared to verify the usefulness of the seat support mechanism in reducing body load. A small EMG value indicated a small physical burden.

### 3.1.2. Verification of physical load reduction

During this experiment, the effectiveness of the proposed seat support mechanism in improving the clarity of US images and reducing body displacement during the examination was quantitatively evaluated and validated. The procedure for the experiment is as follows:

(1) Markers were attached at three locations (the left shoulder, right shoulder, and center of the back) of the patient, which are the reference points from which the motion capture reads the position. The average value of the three markers was taken as the body position of the subject and was continually measured during the examination.

(2) The subject is placed on the robot and the initial position of the robot's probe is manually adjusted to be at the subject's xiphoid process, which is the origin of the coordinates (Figure 11).

(3) The robot automatically moved the probe position (x- and y-axes) and performed a five-way traveling scan on the left chest wall. The US images with the probe position information were collected along the path. The path of the five-way traveling scan is shown in Figure 11, and the probe is moved on this path with the roll, pitch, and yaw angle of the probe fixed at 0°. This path corresponds to those in the heart search method using an automatic echocardiography robot [25]. Figure 10 shows the tool control point, the degrees of freedom of the probe, and the mechanism that moves it.

(4) Images in which the heart was depicted were extracted from a set of US images acquired during the five-way traveling scan. In cases where the heart was visible, the internal structure of the heart was depicted in white and the luminance value was high (Figure 12(a)). However, in cases where the heart was not visible, the heart was depicted in black and the luminance value was low (Figure 12(b)). Thus,
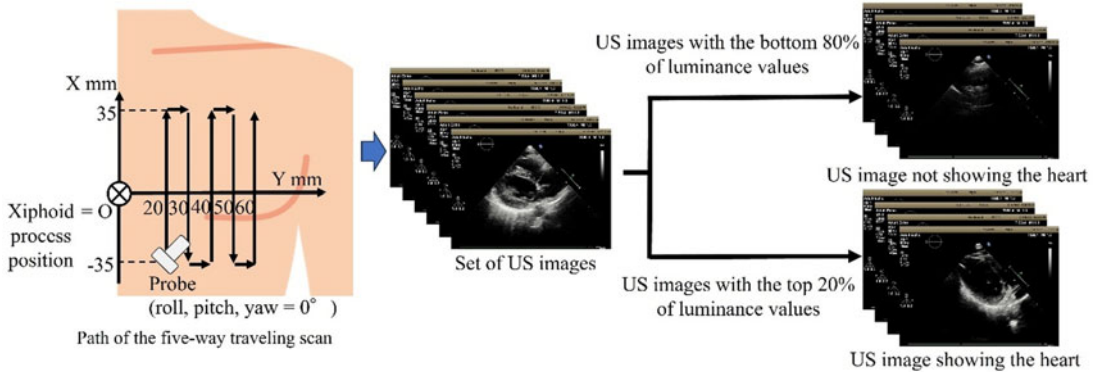
Figure 11. *Overview of process (3) of "Verification of improved clarity of ultrasound images and reduction of body displacement" section.*
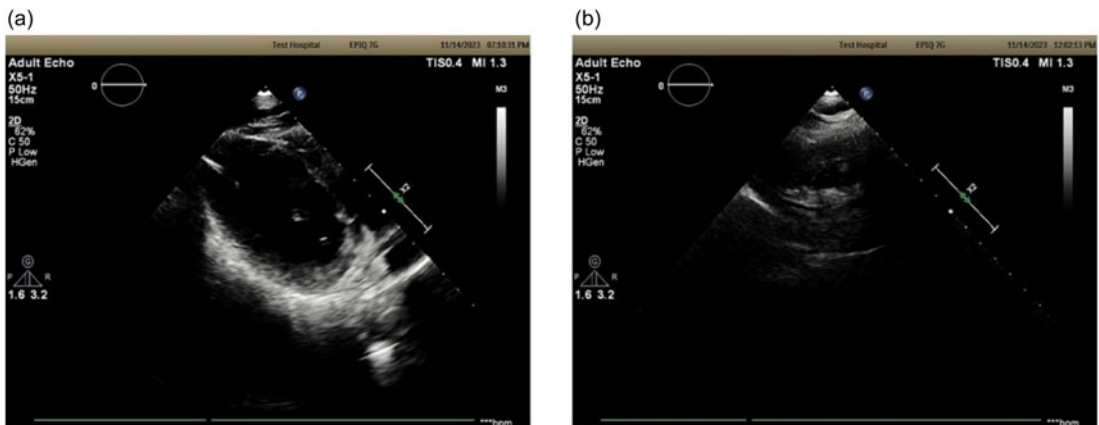
Figure 12. *(a) Difference in ultrasound images depending on whether the heart was visible or (b) not visible.*

images in which the heart was depicted were extracted as those where the total brightness ranked in the top 20% among the US images (Figure 11).

(5) Laplacian filter edge detection was performed on each US image extracted in (4). The average value of all the pixels in the image was calculated and used as the sharpness of the image contour.

(6) The median of the contour sharpness values for each US image calculated in (5) was the representative value of the contour sharpness of the image under each condition.

(7) The mitral valve is detected in a set of images acquired during scanning in the five-way traveling scan, and the maximum value of the confidence score is calculated as a representative value indicating diagnostic accuracy. In a previous study Ref 12, the parasternal long-axis view, which is one of the basic views required for robotic diagnosis, was obtained based on the position of the mitral valve. Thus, in this paper, mitral valve confidence score was used as a representative value of diagnostic accuracy. The confidence score of the mitral valve is calculated using the Yolo v8 model trained with 300 epochs and 8 batch sizes using 7422 images (5938 for training and 1484 for validation) annotated with the mitral valve according to the rule that the mitral valve is not fully closed, as defined by the authors. The mean average precision 50 (mAP50) of this mitral valve object detection model was 0.773.

(8) The number of US images in which the heart can be observed is calculated for the set of US images acquired during scanning in the five-way traveling scan as a representative value of the area range in which the heart can be seen. The criterion for a US image in which the heart is observable is that the
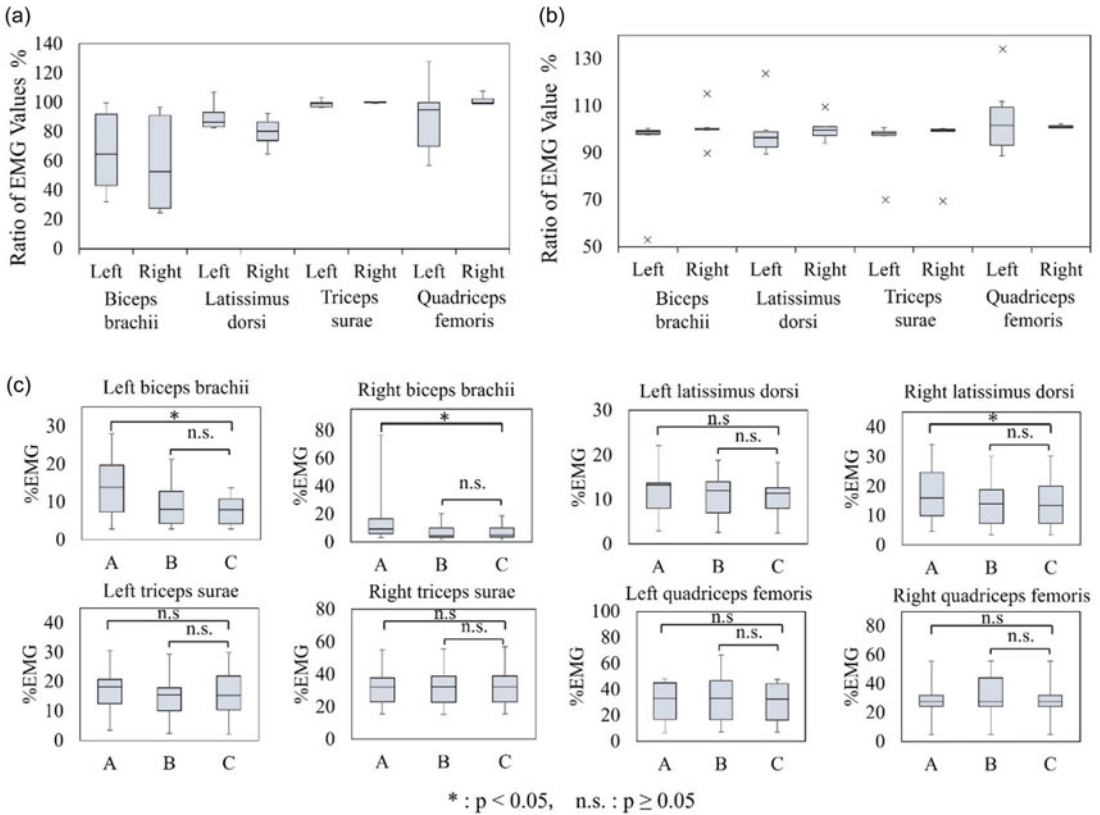
Figure 13. *Ratio of electro myo graph (EMG) values of each site of (a) condition C compared with base condition A, (b) condition C compared with base condition B. (c) %EMG values for each site in each condition.*

myocardium of the heart occupies an angle of about 80% of the fan-shaped area of the US image, and the judgment was made by visually confirming the US image.

(9) Procedures (1)–(8) were conducted once for each condition shown in Table II. The median of the sharpness of the image contour level for each condition, maximum number of confidence score of mitral valve, number of images of the heart that can be observed, and the distance at which the body most deviated from the body position at the start of the five-way traveling scan were compared to verify the validity of the seat support mechanism. A high the sharpness of the image contour level indicates that the image contours are clear.

3.2. Results
3.2.1. Verification of physical load reduction
Figure 13(a) shows the ratio of the EMG values of each site of condition C compared with base condition A. The median values were as follows: left biceps brachii, 64.7%; right biceps brachii, 52.7%; left latissimus dorsi, 86.4%; right latissimus dorsi, 80.2%; left triceps surae, 99.1%; right triceps surae, 99.1%; left quadriceps femoris, 94.9%; and right quadriceps femoris, 99.5%.

Figure 13(b) shows the ratio of the EMG values of each site of conditions C compared with base conditions B. The median values were as follows: left biceps brachii, 98.9%; right biceps brachii, 99.8%; left latissimus dorsi, 96.4%; right latissimus dorsi, 99.6%; left triceps surae, 98.4%; right triceps surae, 98.4%; right triceps surae, 99.3%; left quadriceps femoris, 101.7%; and right quadriceps
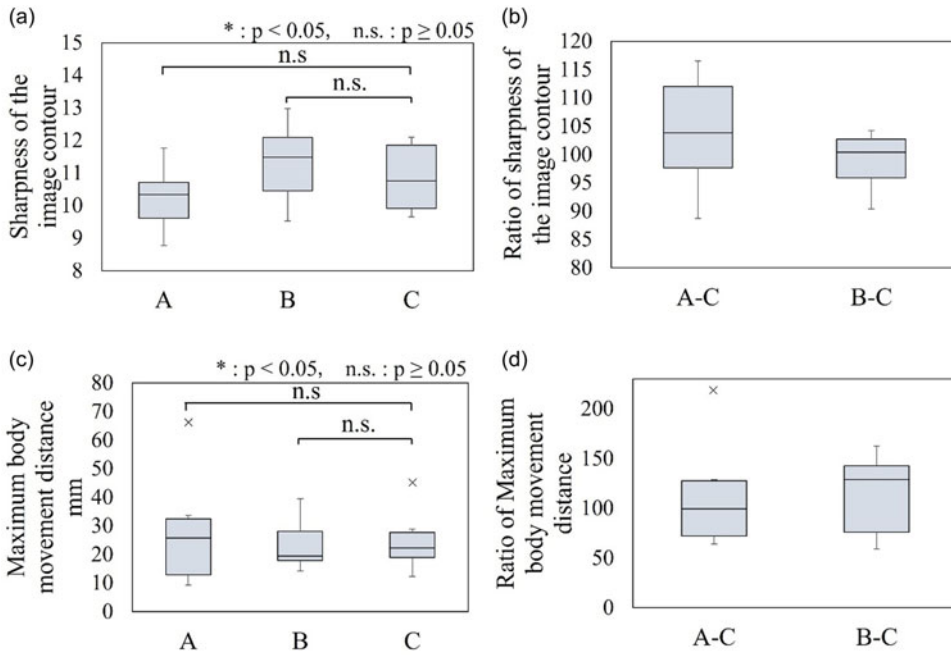
Figure 14. *Verification of improved clarity of ultrasound images and reduction of body displacement. (a) Sharpness of the image contour. (b) Ratio of sharpness of the image contour. (c) Maximum body movement distance during the five-way traveling scan. (d) Ratio of the maximum body movement distance by the body during the five-way traveling scan.*

femoris, 100.9%. Figure 13(c) shows the %EMG values for each site in each condition and the results of the Wilcoxon signed-rank test.

### 3.2.2. Verification of physical load reduction

Figure 14(a) shows the sharpness of the image contour under each condition and the results of the Wilcoxon signed-rank test. Figure 14(b) shows the ratio of the sharpness of the image contour of condition C compared with base condition A and condition C compared with base condition B with medians of 103.8% and 100.4%, respectively. Figure 14(c) shows the maximum distance moved by the body during the five-way traveling scan under each condition and the results of the Wilcoxon signed-rank test. Figure 14(d) shows the ratios of the maximum travel distance during the five-way traveling scan of condition C compared with base condition A and condition C compared with base condition B, which were 99.5% and 128.8%, respectively.

Figure 15(a) shows the confidence score of the mitral valve under each condition and the results of the Wilcoxon signed-rank test. Figure 15(b) shows the ratio of the confidence score of the mitral valve of condition C compared with base condition A and condition C compared with base condition B with medians of 102.7% and 99.8%, respectively. Figure 15(c) shows the number of images in which the heart can be observed under each condition and the results of the Wilcoxon signed-rank test. Figure 15(d) shows the ratios of the number of images in which the heart can be observed of condition C compared with base condition A and condition C compared with base condition B, which were 132.3% and 93.3%, respectively. The relationship between the mitral valve confidence score and US images is also shown in Figure 16.

Table IV shows the EMG for the left and right quadriceps femoris and maximum body movement during the five-way traveling scan percentages decrease of condition C compared with base condition A and condition C compared with base condition B for each subject. Table V shows the sharpness

Table IV. *Percentage decrease resulting of condition C compared with base condition A, and condition C compared with base condition B, for each subject (Other than image quality related).*

Subject	Height cm	Left quadriceps femoris		Right quadriceps femoris		Maximum moving distance	
		A-C %	B-C %	A-C %	B-C %	A-C %	B-C %
a	156	−0.5	−1.6	**−7.7**	−0.6	**−28.5**	41.1
b	163	**−27.8**	**−35.0**	**−3.4**	−2.3	35.9	40.1
c	170	7.9	**−11.9**	1.2	−1.0	28.7	**−33.9**
d	172	2.4	11.4	0.6	−0.6	**−121.7**	**−45.6**
e	182	43.1	−1.8	1.2	−1.5	26.2	**−23.8**
f	188	37.5	9.7	0.3	−0.8	**−25.2**	**−62.4**
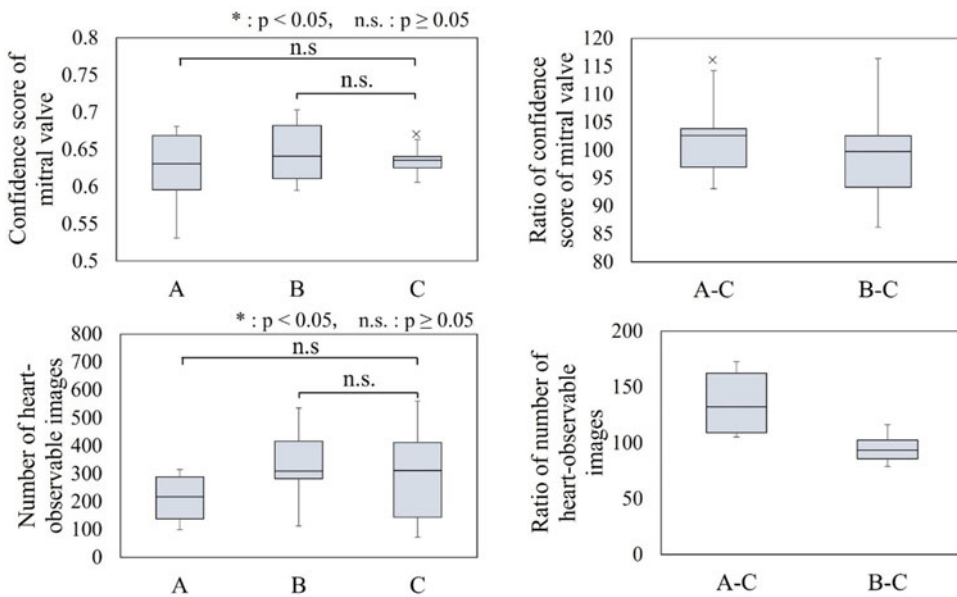
Figure 15. *Verification of improved mitral valve confidence score and improved range of heart observation on ultrasound images. (a) Confidence score of the mitral valve. (b) Ratio of the confidence score of the mitral valve. (c) Number of images in which the heart can be observed. (d) Ratio of the number of images in which the heart can be observed.*
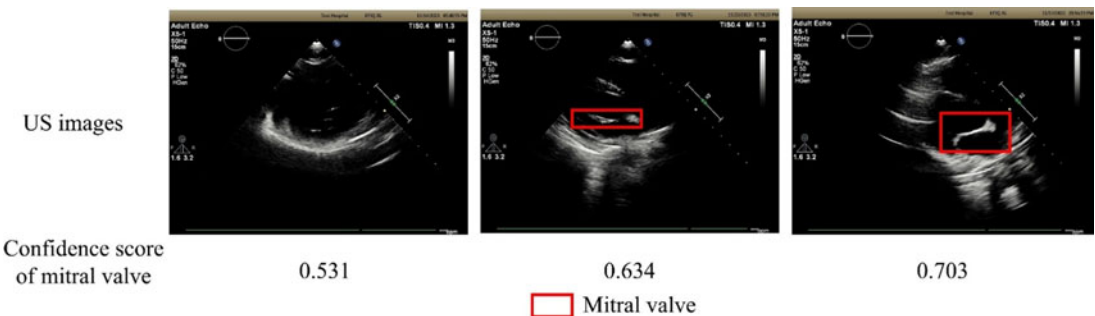
Figure 16. *Relationship between the mitral valve confidence score and ultrasound images.*

Table V. *Percentage increase resulting of condition C compared with base condition A, and condition C compared with base condition B, for each subject (Image quality related).*

| Subject	Height cm	Sharpness of the image contours		Confidence score of mitral valve		Number of images in which the heart can be observed	
		A-C %	B-C %	A-C %	B-C %	A-C %	B-C %
a	156	**−4.2**	1.4	**−4.9**	**−0.3**	27.4	27.4
b	163	3.3	4.3	2.8	12.4	70.9	**−15.6**
c	170	16.5	−0.6	4.3	**−0.2**	3.0	**−9.7**
d	172	14.5	**−5.4**	**−6.9**	**−8.8**	37.1	**−3.6**
e	182	**−11.3**	**−9.6**	2.5	**−13.8**	91.8	4.5
f	188	4.4	3.1	17.3	3.5	**−45.5**	**−75.8**

of the image contour, confidence score of mitral valve, and number of images in which the heart can be observed, along with the percentage increase of condition C compared with base condition A and condition C compared with base condition B for each subject. Tables IV and V show the items that exhibited no improvement using the seat support mechanism. In Table IV and V, those that have not been particularly improved by the seat support mechanism (Left quadriceps femoris, Right quadriceps femoris: less than −3.0%, Maximum moving distance: less than 0.0%, Sharpness of image contours: less than −3.0%, Confidence score of mitral valve and number of images in which the heart can be observed: less than 0.0%) are shown in bold.

3.3. Discussions

The results of verification of physical load reduction suggest that the use of a seat support mechanism can reduce the body load on the arms and lower back while maintaining the load on the legs. Statistically, there were also significant differences in body load on both sides of the arms and on the right side of the back, and no increasing trend was observed in the legs. The reduction of the body load on the arms and lower back is thought to have been caused by the support provided by the normal force from the seat surface of the seat support mechanism to the subject's buttocks. The maintenance of body load on the legs could also contribute to the function of the seat support mechanism to keep the subject's legs grounded perpendicular to the foundation. These results were the same as those derived in Sec.2-2. By fine-tuning parameters, such as the position and angle of the seat support mechanism, according to the height of the individual when using the seat support mechanism, it was possible to reduce the body load on the arms, lower back, and upper thighs, whereas the body load on the lower thighs increased in certain subjects. There were no statistically significant differences in the %MVC values for each site.

As for the validation results regarding the quality of US images to be acquired and the improvement of body displacement, the statistical analysis did not show any significant results of improvement, and it could not be said that these were improved by the seat support mechanism. On the other hand, Tables IV and V indicate that subjects with short and tall stature tend to show less improvement in them by the seat support mechanism.

First, Tables IV and V show that short subjects tend to have increased body loading on the lower legs and body displacement during the examination, and decreased the quality of US images to be acquired. Figure 17 shows a short subject seated on the seated-style echocardiography robot under each condition of the experiment. In regard to the center of gravity of the patient in Figure 17, it is approximately assumed based on the posture model of the patient riding the seat support mechanism, and the position is written in the figure. The angle between upper thigh and horizontal axis $\theta 1$ increased, as shown in Figure 18(c), in the appropriate posture for the short subject identified by this method. Under condition

●Position of the body center of gravity ➡ Normal force of seat ┄➤ Z-axis component of the normal force of seat
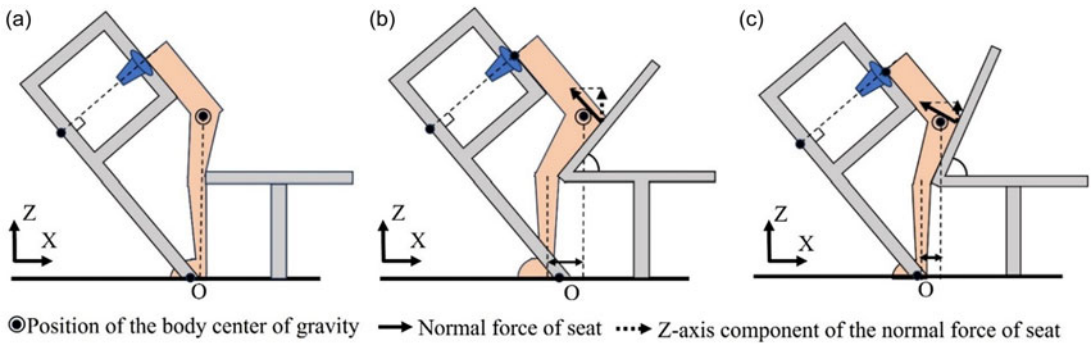
Figure 17. *Short subject seated on the seated-style echocardiography robot under conditions (a) A, (b) B, and (c) C.*
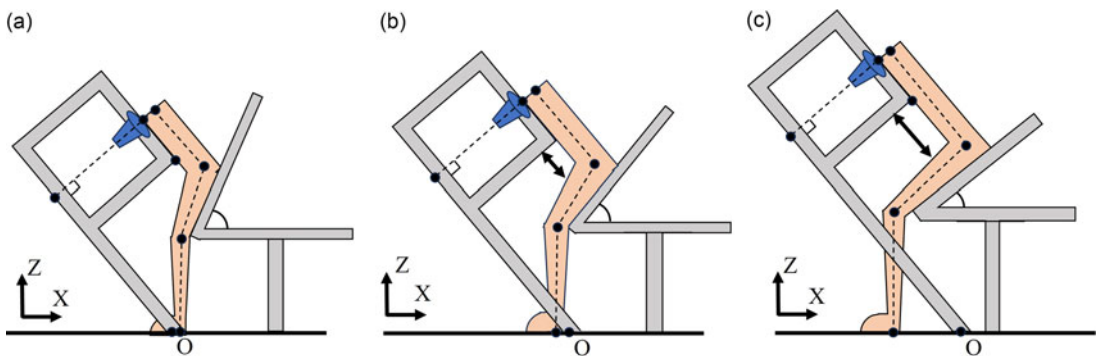
Figure 18. *Relationship between the patient height and the position of the seat support mechanism. (a) Short height. (b) Standard. (c) Tall height.*

A, there was no postural guidance to the lower back and legs by the seat support mechanism; therefore, the leg posture was similar to a standing posture, as shown in Figure 17(a). Thus, the X-coordinate of the body's center of gravity was within the X-coordinate of the sole of the foot, and there was no need to exert force to support the foot to prevent the body from falling. Oppositely, under condition C, the upper thighs were behind the lower thighs because of induction by the seat support mechanism. Therefore, the X-coordinate of the center of gravity was outside the X-coordinate of the sole. Thus, the body needed to be supported with force on the feet to prevent the body from falling backward. This suggested that condition C may have resulted in a higher body load of the quadriceps femoris for the short subjects when comparing conditions A and C.

The inclination angle of the seat surface under condition B exceeded that under condition C (Figure 17(b)). The distance between the X-coordinates of the center of gravity and the sole was larger under condition B. The Z-axis component of the normal force of the seat surface supporting the body on the other hand was greater under condition B. The former and latter are factors that increase or decrease the body load on the legs, respectively. During this verification, the decrease in the body load on the legs due to the latter factor may have been dominant, and the body load of the quadriceps femoris was smaller under condition B than under condition C. The decrease in the sharpness of the image contours was considered to be due to the force exerted on the chest in a direction away from the chest search unit because of the large moment of the body tipping backward caused by these factors. This caused the chest to move away from the probe. Furthermore, it was considered that the moment of the body falling backward caused the body to easily move during the examination. This problem can be solved

by presenting the appropriate posture for short subjects based on a standing posture rather than a sitting posture.

Next, Tables IV and V show that tall subjects tend to have increased body displacement during the examination, and decreased the quality of US images to be acquired. This result may have been due to the large space between the chest search unit and the upper leg of the subject when the tall subject was guided into the proper posture (Figure 18(b) and 18(c)). The space between the chest search unit and upper leg loosened the body constraint, enabling the subject to move their body. This was thought to have likely caused the subject to be in a posture that was out of alignment with the proper posture, causing the chest to move away from the probe and the body to move during the examination. This problem can be solved for tall subjects by installing a mechanism on the robot that bridges the gap between the chest search unit and the upper leg, thereby reducing the deviation from the proper posture.

3.4. Limitations

The seat support mechanism proposed herein, and its verification have several limitations. The first limitation is that in simplifying the modeling of the patient, it was assumed that the ratio of length to width of the glenoid-hip-upper leg-lower leg was constant regardless of the height of the patient. Thus, independent of height, the ratios of the length and width of each body part were assumed to be equivalent to the ratios calculated from the average values calculated from Ref. [27]. Each value was derived from the height of each subject. In reality, the ratio of the length and width of the torso from the joint to the xiphoid process, upper leg, and lower leg varies among individuals. The proposed calculation method may not have been capable of calculating the accurate values and identifying the appropriate posture for the patient. Furthermore, the automatic measurement of the length and width of each body part during an examination using a seated-style echocardiography robot was unrealistic because it requires additional measurement equipment in addition to the robot. Thus, in the future, it is necessary to evaluate the physical load and image clarity when inspections are performed in the appropriate posture for the actual length and width of the patient and the appropriate posture based on the assumptions estimated herein. In addition, it is necessary to verify if the modeling based on assumptions can still demonstrate sufficient physical load and image clarity for inspections.

The second limitation is the limited number of subjects in the validation experiments. We recognize that it is necessary to perform a comparative study on a larger number of subjects with variations in gender, body size, and age. Although we discuss the increased body load on the legs of short/tall subjects and the decreased sharpness of the image contours, the examination was conducted on two short, average-height, and tall subjects each (six in total). Furthermore, since the subjects in this study were males in their 20s, it is possible that they were able to maintain their posture due to the muscular strength of their arms and lower back. In the future, it will be necessary to verify the effectiveness of the seat support mechanism in image acquisition by testing it on subjects with weak muscular strength, such as older people and women. Thus, in the future, it is necessary to examine the proposed seat support mechanism on a larger number of subjects, including short and tall individuals, those with weak muscular strength such as older adults and women, to further analyze the issues.

The third limitation is that the validation time of the physical load was 30 s, which was shorter than the actual expected testing time. Thus, it is necessary to evaluate it over a longer period. We will investigate the relationship between the physical load measured with EMGs and the difficulty of maintaining the posture angle for a long time.

The fourth limitation is the method of conducting the validation study. In the validation test, the number of tests was limited to one so that the physical burden on the patient would not increase and fatigue would not affect the validation results. In the validation test, multiple EMG and US images were obtained, and the median value was derived as the representative value for that validation test, so the reproducibility of the data is considered to be assured, but it is not certain. It is necessary to verify the reproducibility of the present study in the future.

The fifth limitation is that the space between the robot's chest search unit and the seat support mechanism is narrow, making it difficult for obese patients to ride the robot with the seat support mechanism. It is necessary to improve the shape of the chest search unit and widen the space between the chest search unit and the seat support mechanism in the future.

4. Conclusion

The seated-style echocardiography robot performs examinations by adjusting the posture of the patient from a seated position to a rotated or flexed position. However, a challenge exists in that the chest examination and probe scanning areas become misaligned when the posture is bent. This paper proposes a seat support mechanism that guides the patient to an appropriate body position where the chest of the patient fits within the examination range of the chest examination unit while maintaining a low physical load on the patient. Three posture conditions were defined to satisfy the aforementioned conditions. The human body was modeled to derive a posture that satisfies the above conditions for the height of an individual, and the seat support mechanism introducing four DOFs (seat sliding, seat lifting, seat tilting, and probe position-adjusting mechanisms) was installed to guide the user to the derived posture. The EMG values of the left biceps brachii, right biceps brachii, left latissimus dorsi, and right latissimus dorsi were reduced to 64.7%, 52.7%, 86.4%, and 80.2%, respectively, after the introduction of the mechanism. In addition, the sharpness of the image contours was improved to 103.8%. The results suggest that this system can acquire diagnostic images while reducing the physical burden. In the future, we plan to combine a seated-style echocardiography robot equipped with a seat support mechanism and automated testing methods to realize accurate and less burdensome echocardiography examinations.

References

[1] WHO (World Health Organization) (2021). "Cardiovascular diseases (CVDs)." *World Health Organization*. https://www.who.int/news-room/fact-sheets/detail/cardiovascular-diseases-(cvds). Accessed 25 July 2024.

[2] I. Ahmed and N. Sasikumar (2023). "Echocardiography imaging techniques," *National Library of Medicine*. https://www.ncbi.nlm.nih.gov/books/NBK572130/. Accessed 27 September 2024.

[3] N. Koizumi, S. Warisawa, M. Nagoshi, H. Hashizume and M. Mitsuishi, "Construction methodology for a remote ultrasound diagnostic system," *IEEE Trans. Robot.* **25**(3), 522–538 (2009).

[4] P. Abolmaesumi, S. E. Salcudean, Wen-Hong Zhu, M. R. Sirouspour and S. P. DiMaio, "Image-guided control of a robot for medical ultrasound," *IEEE Trans. Robot. Autom.* **18**(1), 11–23 (2002).

[5] K. Ito, S. Sugano and H. Iwata. Portable and attachable tele-echography robot system: FASTele. In: *2010 Annu. Int. Conf. IEEE Eng. Med. Biol. Soc. EMBC'10, 2010*, pp. 487–490 (2010).

[6] A. S. B. Mustafa, T. Ishii, Y. Matsunaga, R. Nakadate, H. Ishii, K. Ogawa, A. Saito, M. Sugawara, K. Niki and A. Takanishi, "Development of robotic system for autonomous liver screening using ultrasound scanning device," *IEEE Int. Conf. Robot. Biomimetics* **2013**, 804–809 (2013).

[7] T.-Y. Fang, H. K. Zhang, R. Finocchi, R. H. Taylor and E. M. Boctor, "Force-assisted ultrasound imaging system through dual force sensing and admittance robot control," *Int. J. Comput. Assist. Radiol. Surg.* **12**(6), 983–991 (2017).

[8] P. Arbeille, J. Ruiz, P. Herve, M. Chevillot, G. Poisson and F. Perrotin, "Fetal tele-echography using a robotic arm and a satellite link," *Ultrasound Obstet. Gynecol* **26**(3), 221–226 (2005).

 [9] J. Esteban, W. Simson, S. Requena Witzig, A. Rienmüller, S. Virga, B. Frisch, O. Zettinig, D. Sakara, Y.-M. Ryang, N. Navab and C. Hennersperger, "Robotic ultrasound-guided facet joint insertion," *Int. J. Comput. Assist. Radiol. Surg.* **13**(6), 895–904 (2018).

[10] S. Wang, D. Singh, D. Johnson, K. Althoefer, K. Rhode and R. J. Housden, "Robotic ultrasound: View planning, tracking, and automatic acquisition of transesophageal echocardiography," *IEEE Robot. Automat. Mag.* **23**(4), 118–127 (2016).

[11] S. Wang, R. J. Housden, Y. Noh, et al., "Analysis of a customized clutch joint designed for the safety management of an ultrasound robot," *Appl. Sci. (Basel)* **9**(9), 1900 (2019).

[12] S. Wang, J. Housden, Y. Noh, et al., "Robotic-assisted ultrasound for fetal imaging: Evolution from single-arm to dual-arm system," *Lect. Notes Comput. Sci.* **11650**, 27–38 (2019).

[13] R. Tsumura and H. Iwata, "Development of ultrasonography assistance robot for prenatal care," *SPIE Med. Imag.* **11315**, 677–684 (2020).

[14] R. Tsumura, J. W. Hardin, K. Bimbraw, A. V. Grossestreuer, O. S. Odusanya, Y. Zheng, J. C. Hill, B. Hoffmann, W. Soboyejo and H. K. Zhang, "Tele-operative low-cost robotic lung ultrasound scanning platform for triage of COVID-19 patients," *IEEE Robot. Autom. Lett.* **6**(3), 4664–4671 (2021).

[15] Y. Shida, R. Tsumura, T. Watanabe, et al., "Heart position estimation based on bone distribution toward autonomous robotic fetal ultrasonography," *Proc. IEEE Int. Conf. Robot. Automat* **2021**, 11393–11399 (2021).

[16] Q. Huang, G.-B. Bian, X.-G. Duan, H.-H. Zhao and P. Liang, "An ultrasound-directed robotic system for microwave ablation of liver cancer," *Robotica* **28**(2), 209–214 (2010).

[17] P. Arbeille, R. Provost, K. Zuj, D. Dimouro and M. Georgescu, "Teles-operated echocardiography using a robotic arm and an internet connection," *Ultrasound Med. Biol.* **40**(10), 2521–2529 (2014).

[18] H. Solvin, S. Sajadi, M. Lippert, R. Massey, H. Holmstrøm, O. Elle, K. Mathiassen and H. Brun, "Feasibility of teleoperated robotic echocardiography – a pilot study," *WFUMB Ultrasound Open* **1**(2), 100018 (2023).

[19] M. Giuliani, D. Szczęśniak-Stańczyk, N. Mirnig, G. Stollnberger, M. Szyszko, B. Stańczyk and M. Tscheligi, "User-centred design and evaluation of a tele-operated echocardiography robot," *Health Technol.* **10**(3), 649–665 (2020).

[20] P. Zhu and Z. Li, "Guideline-based learning for standard plane extraction in 3-D echocardiography," *J. Med. Imag.* **5**(4), 044503 (2018).

[21] S. Dong, G. Luo, K. Wang, S. Cao, Q. Li and H. Zhang, "A combined fully convolutional networks and deformable model for automatic left ventricle segmentation based on 3D echocardiography," *Biomed. Res. Int.* **2018**(1), 1–16 (2018).

[22] M. A. Degel, N. Navab and S. Albarqouni, "Domain and geometry agnostic CNNs for left atrium segmentation in 3D ultrasound," *Med. Image Comput. Comput. Assist. Interv. (MICCAI 2018)* **11073**, 630–637 (2018).

[23] Y. Takachi, K. Masuda, T. Yoshinaga and Y. Aoki, "Development of a support system for handling ultrasound probe to alleviate fatigue of physician by introducing a coordinated motion with robot," *J. Robot. Soc. Jpn.* **29**(7), 634–642 (2011).

[24] Y. Shida, M. Sugawara, R. Tsumura, H. Chiba, T. Uejima and H. Iwata, "Diagnostic posture control system for seated-style echocardiography robot," *Int. J. Comput. Assist. Radiol. Surg.* **18**(5), 887–897 (2023).

[25] Y. Shida, S. Kumagai, R. Tsumura and H. Iwata, "Automated image acquisition of parasternal long-axis view with robotic echocardiography," *IEEE Robot. Autom. Lett.* **8**(8), 5228–5235 (2023).

[26] H. Kino, K. Saisho, T. Miyazoe, et al. *Japanese Body Size Data Book 2004-2006* (Research Institute of Human, Japan, 2008).

[27] L. D.;s Moreira, J. Figueiredo, P. Fonseca, Jão P. Vilas-Boas and C. P. Santos, "Lower limb kinematic, kinetic, and EMG data from young healthy humans during walking at controlled speeds," *Sci. Data* **8**(1), 103 (2021).